



# Role of Chemical Exchange Saturation Transfer and Magnetization Transfer MRI in Detecting Metabolic and Structural Changes of Renal Fibrosis in an Animal Model at 3T

Anqin Li, MD<sup>1</sup>, Chuou Xu, MD, PhD<sup>1</sup>, Ping Liang, MD<sup>1</sup>, Yao Hu, MD<sup>1</sup>, Yaqi Shen, MD, PhD<sup>1</sup>, Daoyu Hu, MD, PhD<sup>1</sup>, Zhen Li, MD, PhD<sup>1</sup>, Ihab R. Kamel, MD, PhD<sup>2</sup>

<sup>1</sup>Department of Radiology, Tongji Hospital, Tongji Medical College, Huazhong University of Science and Technology, Wuhan, China; <sup>2</sup>Russell H. Morgan Department of Radiology and Radiological Science, Johns Hopkins Medical Institutions, Baltimore, MD, USA

**Objective:** To investigate the value of combined chemical exchange saturation transfer (CEST) and conventional magnetization transfer imaging (MT) in detecting metabolic and structural changes of renal fibrosis in rats with unilateral ureteral obstruction (UUO) at 3T MRI.

**Materials and Methods:** Thirty-five Sprague-Dawley rats underwent UUO surgery (n = 25) or sham surgery (n = 10). The obstructed and contralateral kidneys were evaluated on days 1, 3, 5, and 7 after surgery. After CEST and MT examinations, <sup>18</sup>F-labeled fluoro-2-deoxyglucose positron emission tomography was performed to quantify glucose metabolism. Fibrosis was measured by histology and western blots. Correlations were compared between asymmetrical magnetization transfer ratio at 1.2 ppm ( $MTR_{\text{asym}(1.2\text{ppm})}$ ) derived from CEST and maximum standard uptake value ( $SUV_{\text{max}}$ ) and between magnetization transfer ratio (MTR) derived from MT and alpha-smooth muscle actin ( $\alpha$ -SMA).

**Results:** On days 3 and 7,  $MTR_{\text{asym}(1.2\text{ppm})}$  and MTR of UUO renal cortex and medulla were significantly different from those of contralateral kidneys ( $p < 0.05$ ). On day 7,  $MTR_{\text{asym}(1.2\text{ppm})}$  and MTR of UUO renal cortex and medulla were significantly different from those of sham-operated kidneys ( $p < 0.05$ ). The  $MTR_{\text{asym}(1.2\text{ppm})}$  of UUO renal medulla was fairly negatively correlated with  $SUV_{\text{max}}$  ( $r = -0.350$ ,  $p = 0.021$ ), whereas MTR of UUO renal medulla was strongly negatively correlated with  $\alpha$ -SMA ( $r = -0.744$ ,  $p < 0.001$ ).

**Conclusion:** CEST and MT could provide metabolic and structural information for comprehensive assessment of renal fibrosis in UUO rats in 3T MRI and may aid in clinical monitoring of renal fibrosis in patients with chronic kidney disease.

**Keywords:** Chemical exchange saturation transfer; Magnetization transfer imaging; Renal fibrosis; Unilateral ureteral obstruction

## INTRODUCTION

Fibrosis is a common hallmark of many different disorders characterized by the accumulation of extracellular matrix components and is associated with numerous contributors to functional disturbance (1, 2). The presence and severity

of renal fibrosis are the optimal predictors of chronic kidney disease progression (3, 4). Acupuncture biopsy is currently the gold standard for the diagnosis and assessment of fibrosis. Since biopsies are invasive and involve risk of serious complications, non-invasive methods for renal fibrosis assessment are still highly desirable (5).

Received August 29, 2019; accepted after revision December 8, 2019.

This study was supported by the National Natural Science Foundation of China (Grant No.81771801, No.81701657, and No.81571642).

**Corresponding author:** Zhen Li, MD, PhD, Department of Radiology, Tongji Hospital, Tongji Medical College, Huazhong University of Science and Technology, 1095 Jiefang Avenue, Wuhan 430030, China.

• Tel: (86) 13037178109 • Fax: (86) 02783646605 • E-mail: zhenli@hust.edu.cn

This is an Open Access article distributed under the terms of the Creative Commons Attribution Non-Commercial License (<https://creativecommons.org/licenses/by-nc/4.0>) which permits unrestricted non-commercial use, distribution, and reproduction in any medium, provided the original work is properly cited.

Non-invasive magnetic resonance imaging (MRI) can provide useful anatomical and functional information for diagnosis and staging of kidney disease (5). Several advanced MRI techniques, including diffusion-weighted imaging (6, 7), blood oxygenation level-dependent imaging (8, 9), and magnetic resonance spectroscopic imaging (10, 11), have also been used to quantify the microstructural and metabolic changes in renal fibrosis. However, they only investigate one aspect of renal fibrosis. Since management and predictive outcomes of patients with renal fibrosis depend on multiple factors, effective and non-invasive methods are needed for a more comprehensive assessment (1, 5, 12).

Magnetization transfer imaging (MT) is based on the interaction between semi-solid macromolecular protons and free water protons in the tissue. Using non-selective saturation pulse, MT can detect structural macromolecules, such as proteins, lipids, and carbohydrates in an organism (13-15). This technology has been applied in studies of the brain (14, 16), intestines (17), and kidneys (18). Chemical exchange saturation transfer (CEST) is a novel molecular MRI technique. Through selective saturation of solute protons at specific spectral frequencies with low-bandwidth radiofrequency (RF) irradiation, CEST can quantify endogenous mobile proteins and peptide metabolites in millimolar range (19). A recent study showed that asymmetrical magnetization transfer ratio at 1.2 ppm ( $MTR_{asym(1.2ppm)}$ ) can detect changes of CEST contrast of hydroxyl metabolites in murine diabetic nephropathy (DN), which are associated with severity and progression of DN (20).

Currently, the majority of studies on renal fibrosis using MT or CEST are on MRIs with ultrahigh field strength; however, the ability of these sequences to detect renal fibrosis at clinical field strength remains indeterminate. In this study, we hypothesized that MT and CEST provide valuable information on structural molecules and functional mobile metabolites of renal fibrosis, respectively, in unilateral ureteral obstruction (UUO) rats at 3T MRI. We investigated whether the combination of these two imaging techniques can provide comprehensive and complementary information for assessing renal fibrosis.

## MATERIALS AND METHODS

### Animal Model and Experimental Protocol

The experiment was conducted following the Institutional Guidelines of Experimental Animal Care and Use and was approved by the Committee for Animal Experimentation of

Tongji Hospital, Tongji Medical College, Huazhong University of Science and Technology. Thirty-five specific pathogen-free adult male Sprague–Dawley rats (8–10 weeks of age) were obtained from Laboratory Animal Center, Huazhong University of Science and Technology. They had free access to water and standard laboratory chow. UUO was performed according to the method described previously (6). Briefly, surgery was performed under a general anesthetic with 1% sodium pentobarbital solution (0.3 mL/100 g) administered intraperitoneally. After performing skin preparation and disinfection on the left hypochondrium, a paramedian incision was made and the abdominal cavity was opened. The left ureter was carefully isolated using blunt dissection and then permanently ligated twice with 7-0 nylon suture (Non-absorbable Surgical Suture, Huaiyin Medical Equipment Co., Ltd., Huaian, China) at the middle segment. The muscle, fascia and skin were then closed with 4-0 nylon suture (Non-absorbable Surgical Suture). The rats in the control group underwent the same operation as the UUO group, but without ureteral ligation. The rat assignment and the experimental procedure are shown in Figure 1.

### MRI Scan

MRI studies were performed using a 3T horizontal bore imaging system (Discovery 750, GE Healthcare, Milwaukee, WI,

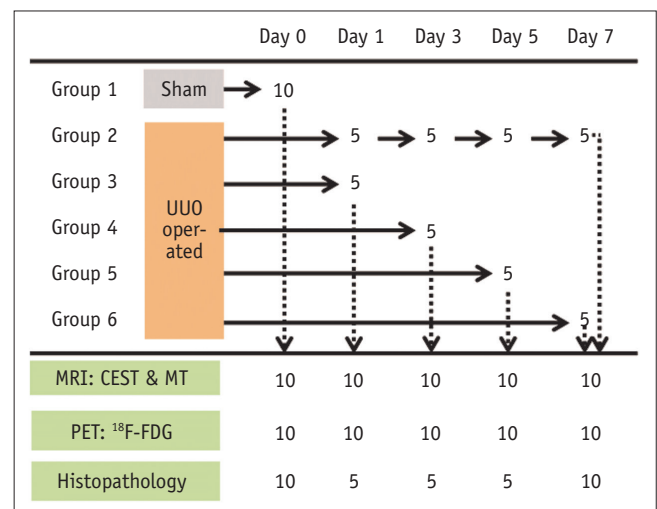


**Fig. 1. Rat assignment and experimental design.** Sham operation was performed in 10 rats of group 1 and UUO operation was performed in 25 rats of groups 2–6. Each group of rats underwent postoperative MRI, followed by corresponding postoperative PET, and finally histopathological examination. Group 2 was followed up on days 1, 3, 5, and 7 after surgery and groups 3–6 were cross-sectionally studied at each time point. CEST = chemical exchange saturation transfer, MRI = magnetic resonance imaging, MT = magnetization transfer imaging, PET = positron emission tomography, UUO = unilateral ureteral obstruction, <sup>18</sup>F-FDG = <sup>18</sup>F-labeled fluoro-2-deoxyglucose

USA). A custom-designed 50-mm-diameter transceiver coil was used to improve the image quality in rats. Before the scan, anesthesia was induced by intraperitoneal injection of 1% sodium pentobarbital solution (0.3 mL/100 g). The imaging protocol consisted of coronal fast-recovery fast spin-echo T2-weighted imaging (T2WI), transverse T1-weighted imaging (T1WI) and T2WI. The acquired routine images were used as anatomical references for CEST and MT scanning localization.

The Z-spectrum, which passes through the largest cross section of renal hilum on both sides, was collected to construct asymmetrical magnetization transfer ratio ( $MTR_{asym}$ ) and magnetization transfer ratio (MTR) maps. Scanning was based on a pseudo-continuous wave RF irradiation with four 400 ms pulses at 2  $\mu$ T amplitude. The acquisition parameters were as follows: repetition time/echo time, 3000/34 ms; slice thickness, 3 mm; field of view, 80  $\times$  80 mm; matrix, 128  $\times$  128; number of excitations, 2. The saturation frequencies were: 0,  $\pm$  0.25,  $\pm$  0.5,  $\pm$  0.75,  $\pm$  1,  $\pm$  1.5,  $\pm$  2,  $\pm$  2.5,  $\pm$  3,  $\pm$  3.25,  $\pm$  3.5,  $\pm$  3.75,  $\pm$  4,  $\pm$  4.5,  $\pm$  5,  $\pm$  6, and +15.6 ppm. An unsaturated image ( $S_0$ ) was acquired for signal normalization. The data acquisition time was 3 minutes 18 seconds.

### MRI Data Analysis

All data were transferred to an AW4.6 Workstation (GE Healthcare) and analyzed using its Functool software. The raw data were first organized into the Z-spectrum. Then, the Z-spectrum was fitted on a pixel-by-pixel basis according to the procedure described previously (16, 21), and the  $B_0$  inhomogeneity map was created. The original Z-spectrum was then corrected for the  $B_0$  inhomogeneity effect through interpolation and centering of the Z-spectrum.

CEST contrast of hydroxyl metabolites was quantified at +1.2 ppm using interpolation method and MTR asymmetry analysis with respect to the water frequency (20).

$$MTR_{asym}(\Delta\omega) = \frac{S(-\Delta\omega)}{S_0} - \frac{S(\Delta\omega)}{S_0} \quad [1]$$

Where  $S(\Delta\omega)$  and  $S(-\Delta\omega)$  were the signals at positive offset and its counterpart at negative offset, respectively.

The MT effect from immobile macromolecules was calculated at +15.6 ppm saturation offset (16).

$$MT = \frac{S_0 - S_{saturation}}{S_0} \quad [2]$$

The cortical and medullary regions of interest (ROIs) were manually segmented based on the original saturated images

at 15.6 ppm that showed the best contrast between the cortex and the medulla. The same ROIs were propagated to the reconstructed  $MTR_{asym(1.2ppm)}$  and MTR maps, and parameter values for each kidney cortex and medulla were obtained.

### Positron Emission Tomography Acquisition and Image Processing

Imaging with  $^{18}$ F-labeled fluoro-2-deoxyglucose positron emission tomography ( $^{18}$ F-FDG PET) was conducted using a high-resolution, dedicated, small-animal PET system (Trans-PET BioCaliburn 700, Raycan Technology Co., Ltd., Suzhou, China). Rats were kept under anesthesia (1.5%/98.5% isoflurane/oxygen mixture) throughout the experiment. The rats were injected with 446–520  $\mu$ Ci fluorodeoxyglucose via the lateral tail vein, and a dynamic PET scan was started immediately, the scan took 30 minutes to complete.

Three-dimensional ROIs were manually drawn over the entire kidney. The standard uptake value (SUV) was measured in each ROI using the following formula:

$$SUV = \frac{\text{Voxel radioactivity (MBq/mL)}}{\text{Injected dose (MBq/mL)} \times \text{Rat Weight (g)}} \quad [3]$$

The maximum SUV ( $SUV_{max}$ ) was selected as the reference standard for glucose uptake and metabolic activity in each kidney.

### Blood Test

The concentrations of serum creatinine and blood urea were determined using an automated multi-parametric biochemical analyzer (Cobas c701, Roche Diagnostics GmbH, Penzberg, Germany).

### Histologic Evaluation

Kidney tissues fixed in formalin were paraffin-embedded and cut into 3- $\mu$ m-thick coronal sections and stained with hematoxylin and eosin (H&E) and Masson trichrome staining (MTS). Renal histological changes and collagen deposition were assessed by an experienced nephropathologist.

### Immunohistochemical Staining and Western Blot Analysis

To analyze the protein localization expression of alpha-smooth muscle actin ( $\alpha$ -SMA), immunohistochemical staining was performed as previously described (22). Western blotting was used to quantify  $\alpha$ -SMA content. The intensities of individual bands were quantified by

densitometry using Image J (National Institutes of Health Bethesda, MD, USA) and normalized to the  $\beta$ -actin level. Please refer to Zhao et al. (23) for more details.

### Statistical Analysis

ANOVA was used to compare  $MTR_{\text{asym}(1.2\text{ppm})}$ , MTR, and  $SUV_{\text{max}}$ , and creatinine, urea, and  $\alpha$ -SMA content among multiple time points. At each time point after ligation, paired Student's *t* tests were performed to identify differences in  $MTR_{\text{asym}(1.2\text{ppm})}$  or MTR values between UUO and contralateral (CL) sides. Pearson correlation coefficient (*r*) was used to assess the relationship between  $SUV_{\text{max}}$ ,  $\alpha$ -SMA, and MRI parameters. Statistical analyses were carried out using SPSS (version 19.0, IBM Corp., Armonk, NY, USA) and results with  $p < 0.05$  were considered statistically significant.

## RESULTS

### Animal Characteristics, Morphological, and Histologic Assessment

The animal weight and renal function indexes are shown in Table 1. The blood urea levels of UUO rats on days 1, 3, and 7 after ligation were increased significantly when compared with the sham-operated group ( $p$  values: 0.001,  $< 0.001$ , and  $< 0.001$ , respectively).

Figure 2A shows representative images of coronal T2WI of sham-operated and UUO rats. Urine collected within the renal pelvis of UUO kidney on day 1 after surgery. Gradually, with the obstruction time prolonged, the volume of UUO kidneys became larger, renal pelvis expanded, and renal parenchyma became thinner due to the irreversible and persistent pressure of hydronephrosis. As a result, the entire kidney became a thin-walled capsule.

Upon serial H&E and MTS staining of the UUO renal tissue (Fig. 2B, C) tubular dilation was observed from day 1; on day 3, glomerular capsules were slightly dilated, tubular dilatation was still obvious, and a small amount of blue staining collagen fibers was present in the renal interstitium; on day 5, parts of renal tubules collapsed

and interstitial blue staining enhanced; and on day 7, glomerular capillaries and renal tubules atrophied and glomerular capsules were clearly dilated. The renal interstitial fibrous structures increased significantly and gradually replaced the normal renal structures.

### $MTR_{\text{asym}(1.2\text{ppm})}$ and MTR Changes in UUO Kidney

Representative images of transverse T1WI and T2WI,  $MTR_{\text{asym}(1.2\text{ppm})}$ , and MTR measurements of sham-operated and UUO rats are shown in Figure 3A-D. When compared with CL kidneys, the cortical  $MTR_{\text{asym}(1.2\text{ppm})}$  of UUO kidneys was significantly higher on days 1, 3, 5, and 7 ( $p$  values: 0.032, 0.037, 0.036, and 0.003, respectively), and the medullary  $MTR_{\text{asym}(1.2\text{ppm})}$  of UUO kidneys was significantly higher on days 3 and 7 ( $p$  values: 0.001 and 0.032, respectively), while no significant difference was noted on days 1 and 5 ( $p$  values: 0.785 and 0.752, respectively) (Fig. 3E). Both the cortical and medullary MTRs of UUO kidneys were significantly lower on days 1, 3, 5, and 7 when compared with CL kidneys (cortex:  $p$  values:  $< 0.001$ ,  $< 0.001$ ,  $< 0.001$ , and 0.001, respectively; medulla:  $p$  values:  $< 0.001$ , 0.001,  $< 0.001$ , and  $< 0.001$ , respectively) (Fig. 3F).

Compared with sham kidneys,  $MTR_{\text{asym}(1.2\text{ppm})}$  in UUO kidneys cortex increased slightly on days 1 (22.9%,  $p = 0.580$ ) and day 3 (76.7%,  $p = 0.069$ ), but then decreased on day 5 (14.0%,  $p = 0.737$ ), and increased again on day 7 (104.5%,  $p = 0.017$ ). Similarly, medullary  $MTR_{\text{asym}(1.2\text{ppm})}$  increased slightly on day 1 (167.7%,  $p = 0.122$ ), increased significantly on day 3 (370.7%,  $p = 0.001$ ), decreased on day 5 (35.0%,  $p = 0.744$ ), and increased again on day 7 (308.5%,  $p = 0.007$ ) (Fig. 3E). Slight reductions in MTR showed up in cortex (14.6%,  $p = 0.019$ ) and medulla (16.2%,  $p = 0.003$ ) of UUO kidney on day 1 and significant reductions were seen on days 3, 5, and 7 (cortex: 23.5%,  $p < 0.001$ ; 28.6%,  $p < 0.001$ ; and 25.4%,  $p < 0.001$ , respectively; and medulla: 23.7%,  $p < 0.001$ ; 25.1%,  $p < 0.001$ ; and 29.9%,  $p < 0.001$ , respectively) (Fig. 3F).

### Estimation of Kidney Glucose Metabolism by $^{18}\text{F}$ -FDG PET

Representative  $^{18}\text{F}$ -FDG PET images of sham-operated

**Table 1. Animal Characteristics and Renal Function Indices**

Indices	Baseline/Sham Group*	Day 1	Day 3	Day 5	Day 7
Weight (g)	209.7 $\pm$ 7.2	212.9 $\pm$ 6.5	218.3 $\pm$ 12.9	206.8 $\pm$ 24.4	202.9 $\pm$ 25.8
Creatinine ( $\mu\text{mol/L}$ )	20 $\pm$ 3	23 $\pm$ 8	24 $\pm$ 9	31 $\pm$ 18	29 $\pm$ 11
Urea (mmol/L)	5.03 $\pm$ 1.00	8.16 $\pm$ 1.42 <sup>†</sup>	9.89 $\pm$ 3.17 <sup>†</sup>	6.84 $\pm$ 1.59	9.27 $\pm$ 1.72 <sup>†</sup>

Data are mean values  $\pm$  standard deviations. \*Weight compared with baseline; creatinine and urea compared with sham-operated rats, <sup>†</sup> $p < 0.05$ .

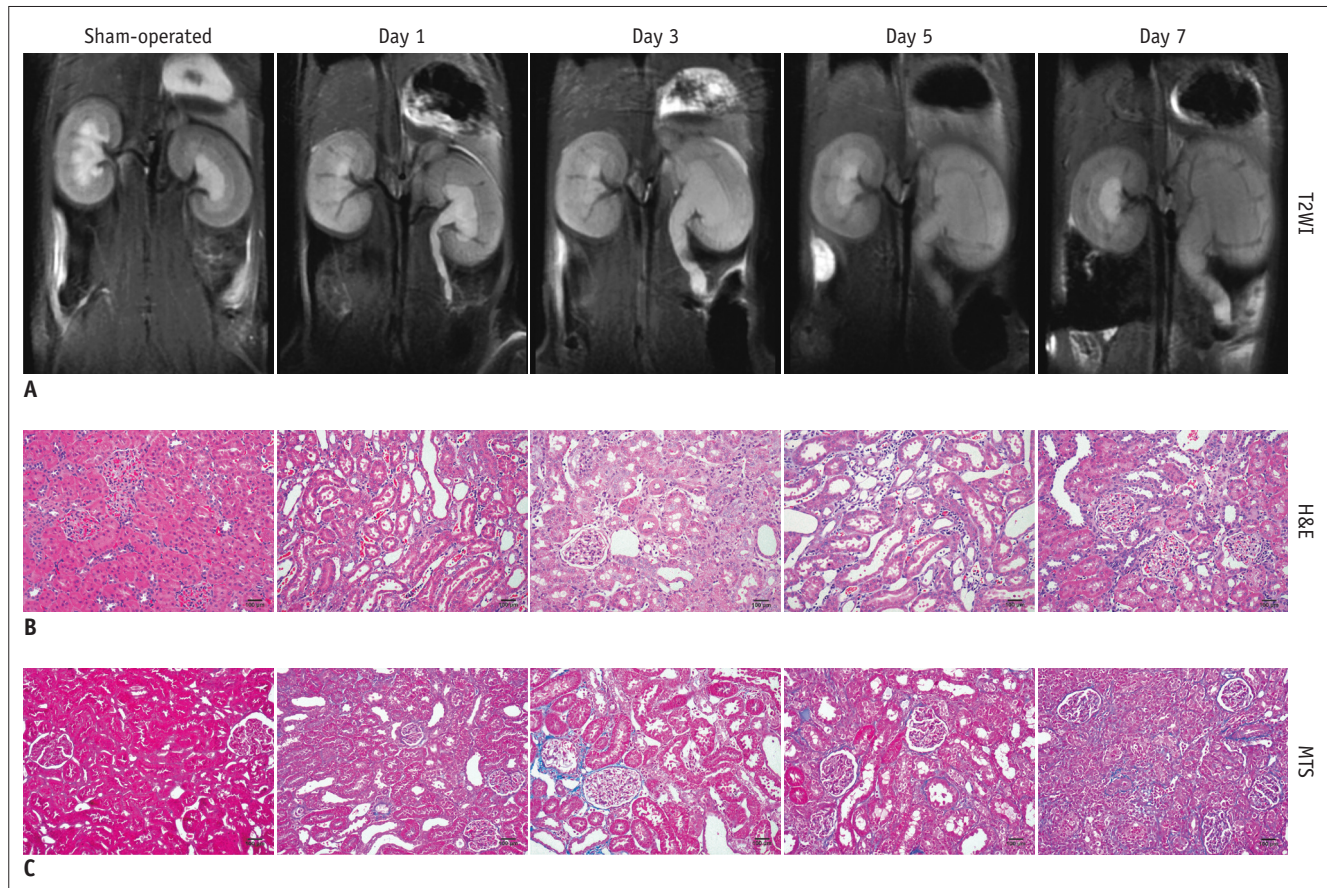


**Fig. 2. Representative coronal T2WI, H&E, and MTS images at each time point after surgery.**

**A.** Images of T2WI show that accumulation of urine within UUO kidney, and corticomedullary contrast is weakened. When obstruction time prolongs, UUO kidney gradually becomes larger and renal parenchyma becomes thinner. **B.** H&E staining demonstrates that UUO kidneys' glomerular atrophy, tubular dilation, tubular atrophy, necrosis, and increased inflammatory cell infiltration. Interstitial space is expanded by matrix deposition and inflammatory cell infiltration (original magnification, x 200). **C.** MTS images show that percentage of blue area representing fibrosis is gradually increasing during subsequent follow-up (original magnification, x 200). H&E = hematoxylin and eosin, MTS = Masson trichrome staining, T2WI = T2-weighted imaging

and UUO rats are shown in Figure 4A. UUO kidneys showed significantly lower  $SUV_{max}$  when compared with CL kidneys on days 1, 3, 5, and 7 ( $p$  values: < 0.001, 0.001, 0.005, and < 0.001, respectively). In comparison to sham kidneys,  $SUV_{max}$  of UUO kidneys decreased significantly on days 1, 3, 5, and 7 (66.8%,  $p$  < 0.001; 59.3%,  $p$  < 0.001; 80.7%,  $p$  < 0.001; and 81.1%,  $p$  < 0.001, respectively), but the extent of decline was attenuated on day 3 (Fig. 4B).

#### Correlations between $MTR_{asym(1.2ppm)}$ and $SUV_{max}$

$MTR_{asym(1.2ppm)}$  was significantly (and negatively) correlated with  $SUV_{max}$  in UUO renal medulla ( $r = -0.350$ ,  $p = 0.021$ ), but not in renal cortex ( $r = -0.279$ ,  $p = 0.070$ ) (Table 2).

#### Evaluation of Renal Fibrosis by $\alpha$ -SMA

Alpha-SMA was expressed in the smooth muscle cells of renal arterioles but was rarely evident in the renal

interstitium of normal kidneys. Ureteral obstruction leads to gradual increase in the interstitial positive staining area of  $\alpha$ -SMA (Fig. 5A). Consistent with these observations, quantitative western blot analysis showed that the expression of  $\alpha$ -SMA in obstructed kidneys increased gradually (Fig. 5B).

#### Correlations between MTR and $\alpha$ -SMA

MTR displayed a negative correlation with  $\alpha$ -SMA expression in UUO renal cortex ( $r = -0.510$ ,  $p = 0.005$ ) and medulla ( $r = -0.744$ ,  $p < 0.001$ ) (Table 2).

## DISCUSSION

The cortical and medullary  $MTR_{asym(1.2ppm)}$  of UUO kidneys were significantly higher than those of CL kidneys on days 3 and 7. Since  $MTR_{asym(1.2ppm)}$  is related to the composition of

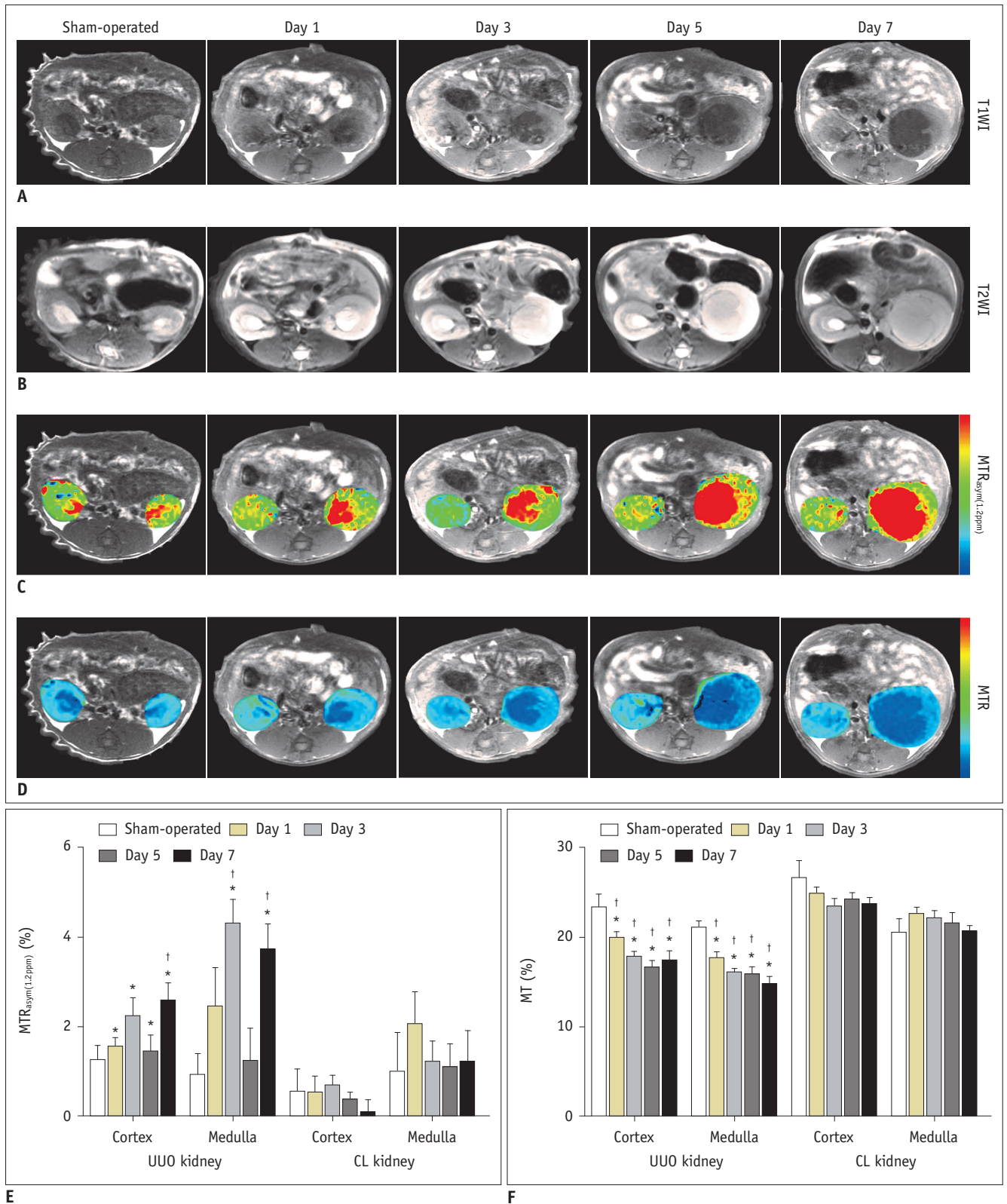


**Fig. 3. Representative images of transverse T1WI and T2WI, MTR<sub>asy(1.2ppm)</sub>, and MTR maps at each time point after surgery. (A) T1WI, (B) T2WI, (C) MTR<sub>asy(1.2ppm)</sub>, and (D) MTR maps of sham-operated rats and UUO rats at 1, 3, 5, and 7 days after obstruction. Blue indicates lowest value, and green, yellow, and red indicate increasing values. E, F. Bar graphs show MTR<sub>asy(1.2ppm)</sub> and MTR quantified in cortex and medulla of all groups. Data show mean ± standard error of mean. \**p* < 0.05 versus CL kidneys, †*p* < 0.05 versus sham-operated kidneys. CL = contralateral, MTR = magnetization transfer ratio, MTR<sub>asy(1.2ppm)</sub> = asymmetrical magnetization transfer ratio at 1.2 ppm, T1WI = T1-weighted imaging**

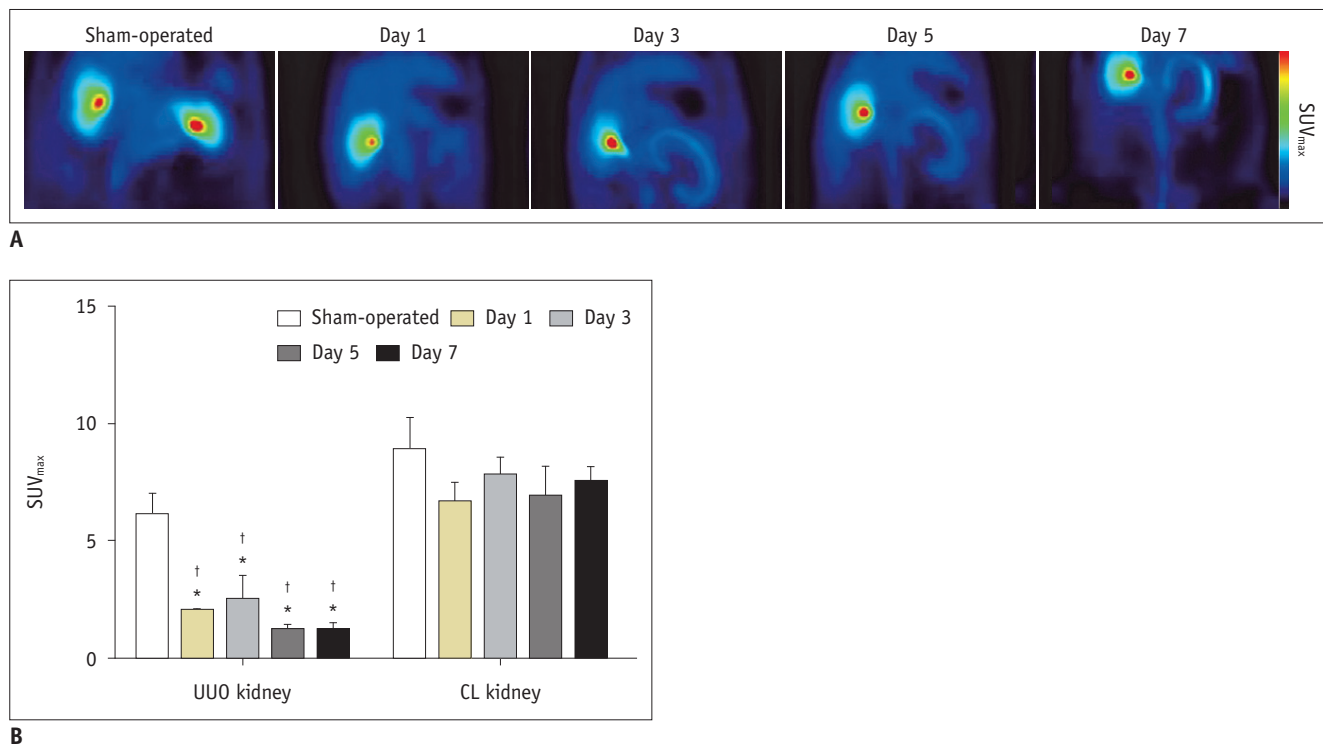


**Fig. 4. Images of <sup>18</sup>F-FDG PET and quantification of FDG metabolism at each time point after surgery.**

**A.** Representative PET images of sham-operated rats and UUO rats at 1, 3, 5, and 7 days after obstruction. Blue indicates lowest value, and green, yellow, and red indicate increasing values. **B.** Bar graphs show renal glucose metabolism quantified by SUV<sub>max</sub> in sham-operated, UUO, and CL kidneys of all groups. Data show mean ± standard error of mean. \**p* < 0.05 versus CL kidneys, †*p* < 0.05 versus sham-operated kidneys. FDG = fluorodeoxyglucose, SUV<sub>max</sub> = maximum standard uptake value

**Table 2. Correlations of MTR<sub>asym(1.2ppm)</sub> and MTR with Glucose Metabolism SUV<sub>max</sub> and Fibrosis Marker α-SMA**

Indicators	MTR <sub>asym(1.2ppm)</sub>				MTR			
	Cortex		Medulla		Cortex		Medulla	
	<i>r</i>	<i>P</i>	<i>r</i>	<i>P</i>	<i>r</i>	<i>P</i>	<i>r</i>	<i>P</i>
SUV <sub>max</sub>	-0.279	0.070	-0.350	0.021	0.555	< 0.001	0.564	< 0.001
α-SMA	0.558	0.002	0.450	0.014	-0.510	0.005	-0.744	< 0.001

MTR = magnetization transfer ratio, MTR<sub>asym(1.2ppm)</sub> = asymmetrical magnetization transfer ratio at 1.2 ppm, SUV<sub>max</sub> = maximum standard uptake value, α-SMA = alpha-smooth muscle actin

hydroxyls, mainly from glucose or glycogen, it indicated that glucose/glycogen content is increased in UUO kidneys (20). These results were not consistent with previous studies (20, 24). Wang et al. (24) reported that UUO kidneys' medulla showed evident amplitude changes for CEST effects at RF offset around 1.2 ppm compared to those of CL kidneys, but the cortex did not show significant amplitude change. In a pathological state, the polarity of renal tubular epithelial cells is destroyed, resulting in abnormal renal tubular transport function. Since the proximal tubular epithelial cells play an important role in reabsorbing glucose in the urine, the transport dysfunction often leads to obstacles to reabsorption of glucose (20, 25). In addition, the difference in results may be due to different acquisition parameters.

MTR<sub>asym</sub> may be contaminated by water longitudinal relaxation time (T<sub>1w</sub>) (26). In our study, we used clinical field strength and shorter RF irradiation time. Zu (27) showed that MTR<sub>asym</sub> is not sensitive to T<sub>1w</sub> at low fields and non-steady-state acquisitions. Therefore, MTR<sub>asym</sub> metric may be more accurate after choosing appropriate sequence parameters.

MTR<sub>asym(1.2ppm)</sub> in UUO kidneys cortex increased significantly on day 7, while the medullary MTR<sub>asym(1.2ppm)</sub> began to show a significant increase on day 3. It suggested that changes in tissue glucose metabolites occurred earlier in medulla than cortex. Previous studies have supported this finding (20, 24). Wang et al. (20) reported that both mild to moderate and advanced DN mice showed higher MTR<sub>asym</sub> in the

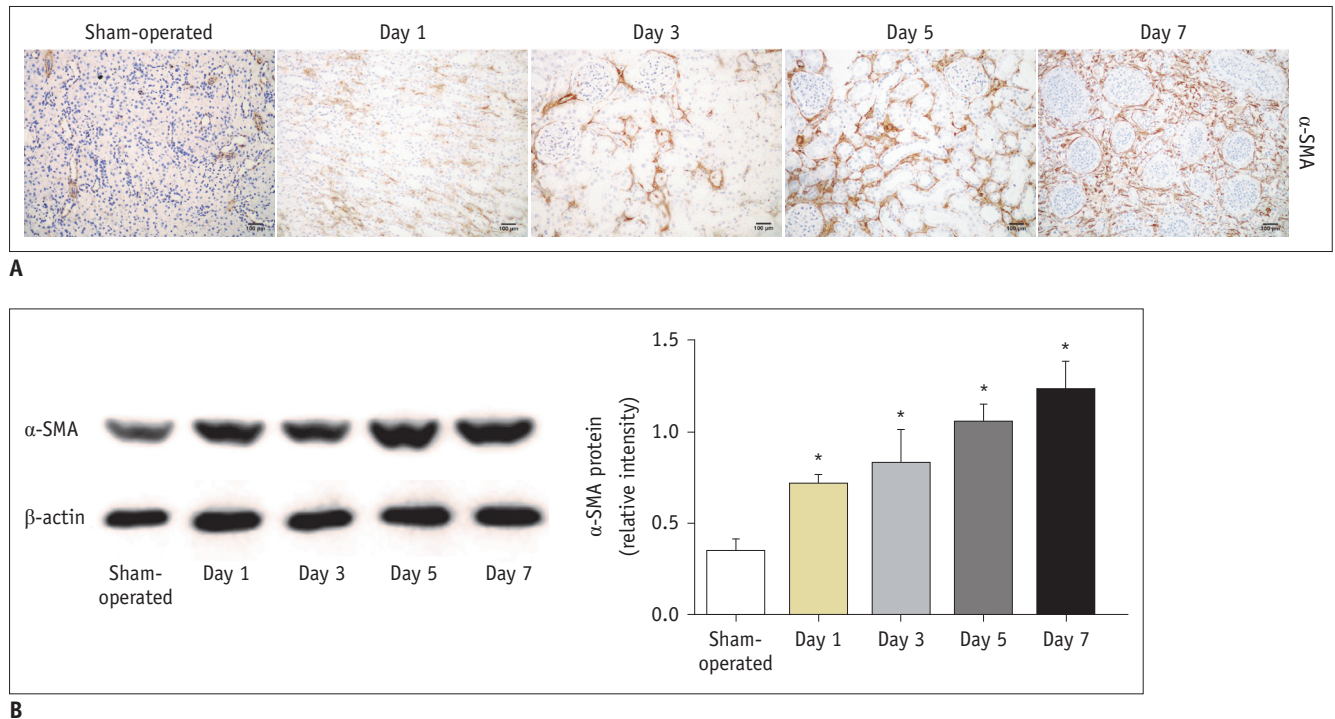


**Fig. 5. Expression of  $\alpha$ -SMA in sham-operated kidneys and UUO kidneys at each time point.**

**A.** Representative images of immunohistochemical staining for  $\alpha$ -SMA (original magnification,  $\times 200$ ).  $\alpha$ -SMA was expressed in renal artery smooth muscle cells of sham-operated kidneys, cytoplasm of some tubular epithelial cells, and interstitial cells of UUO kidneys; expression levels gradually increased. **B.**  $\alpha$ -SMA protein levels were detected by western blotting. Expression levels of  $\alpha$ -SMA were quantified by densitometry and normalized with  $\beta$ -actin. Data show mean  $\pm$  standard error of mean. \* $p < 0.05$  versus sham-operated kidneys.  $\alpha$ -SMA = alpha-smooth muscle actin

medulla at 1.2 ppm RF offset compared with non-diabetic mice. The increased  $MTR_{\text{asym}}$  was also observed in the renal cortex of advanced DN mice. In kidney, CEST effects could be produced by metabolites in blood, urine, and cellular and interstitial components. Pathological changes in various animal models of kidney disease, such as tubular dilation and atrophy and interstitial fibrosis affect the reabsorption of glucose by tubules, especially in the inner medulla (20, 25). In addition,  $MTR_{\text{asym}(1.2\text{ppm})}$  in UUO kidneys increased on day 3, decreased on day 5 and then increased again on day 7. We speculate that the predominant specific physiological and pathological events may be different at each time point in the progression of kidney disease. From day 1 to day 3, tubular dilation was associated with urine retention after UUO. This may cause an increase in  $MTR_{\text{asym}(1.2\text{ppm})}$ . UUO kidneys still had partial reabsorption and compensatory capacity on day 5, resulting in a decrease in  $MTR_{\text{asym}(1.2\text{ppm})}$ . From day 5 to day 7, urine retention and reabsorption disorder became more severe. These changes led to a further increase in  $MTR_{\text{asym}(1.2\text{ppm})}$  (24).

The usefulness of  $^{18}\text{F}$ -FDG PET imaging is based on the correlation with glucose metabolism, and has been extensively studied and applied in the fields of oncology

and inflammatory diseases (28-30). In our study, we observed the correlation between  $MTR_{\text{asym}(1.2\text{ppm})}$  and  $SUV_{\text{max}}$  in the medulla of UUO kidneys and revealed that  $MTR_{\text{asym}(1.2\text{ppm})}$  is associated with glucose metabolism in renal physiology and pathology (12). A study showed that PET pattern in obstructive hydronephrosis was linearly correlated with hydronephrosis severity (31). Inflammatory cell infiltration may increase metabolic activity, while glomerular filtration damage may reduce  $^{18}\text{F}$ -FDG uptake (32, 33). CEST is a noninvasive MRI method based on endogenous mobile molecules. Unlike PET, CEST imaging does not involve ionizing radiations, and could be repeated as necessary for assessing renal metabolites.

In the current study, the cortical and medullary MTRs of UUO kidneys were significantly lower than those of CL kidneys on days 1, 3, 5, and 7, indicating that the semi-solid immobile macromolecules content in UUO kidneys had reduced (14, 24). Wang et al. (24) reported that UUO kidneys showed a significant decrease in MT parameters pool size ratio (the ratio of the macromolecular proton pool to the free water pool) in renal cortex and medulla, compared to CL kidneys. This may be associated with tubular dilation, atrophy and apoptosis in local tissues of UUO kidneys.



Apoptosis leads to the breakdown of membranes and proteins, which alters the level of macromolecules in the kidney microstructure.

This longitudinal study demonstrated that MTR significantly decreased in cortex and medulla of UUO kidneys from day 1 to day 7, while renal cortex showed a slight increase on day 7. Some previous studies had similar observations (15, 24). Wang et al. (24) reported that the pool size ratio in cortex showed dynamic changes and decreased significantly from day 1 to day 6 after UUO surgery. Jiang et al. (15) reported that renal cortex MTR showed a progressive increase initially, followed by a slight decrease during the later period of unilateral renal artery stenosis. The predominant specific pathological events may be different at each stage of kidney disease progression, thus resulting in a decrease or increase of MRI signals. Tubular dilation, atrophy, and denudation of basement membrane at an early stage of obstruction may reduce the pool size ratio. Fibrotic structures replacing the normal renal tissue at a later period of obstruction may increase the pool size ratio (24).

Our study found that MTR of UUO renal cortex and medulla displayed negative correlations with the fibrosis marker  $\alpha$ -SMA, revealing that the reduction in UUO kidney structural macromolecules is accompanied by aggravation of fibrosis. Our findings are different from previously published MT analysis results (15, 18). Jiang et al. (18) previously reported that renal fibrosis quantified from Sirius-red-stained tissue sections showed good positive correlations with MTR at both 600 Hz and 1000 Hz. In UUO kidneys, factors that may affect MTR other than fibrosis, include reduced renal perfusion and accumulation of other extracellular proteins (15).

There are several limitations to this study. First of all,  $MTR_{\text{asym}}$  can provide a quick way to determine the CEST effect. Although asymmetric analysis works well as a first approximation,  $MTR_{\text{asym}}$  measure would be subject to contamination by the asymmetry of MT and upfield nuclear Overhauser enhancement effects in the tissue. Therefore, in order to quantify CEST more accurately, we plan to use a more complicated imaging acquisition or analysis method in the future (16, 20, 26, 34). Secondly, due to technical limitations and restricted scanning time, CEST and MT were scanned in a single representative slice in this study, therefore, MRI signal changes in other regions of the kidney could not be assessed. Thirdly, ROI was delineated only in the cortex and medulla, because renal parenchyma

becomes thinner during the later stages of obstruction and distinguishing between inner and outer medulla becomes difficult. Optimization of MRI sequences may require higher spatial resolution to improve the precision and accuracy of CEST imaging.

In conclusion, CEST and MT have a certain correlation with renal glucose metabolism as measured by  $^{18}\text{F}$ -FDG PET and fibrosis quantified by  $\alpha$ -SMA in UUO rats.  $MTR_{\text{asym}(1.2\text{ppm})}$  and MTR could reflect changes in tissue metabolism and structure of renal fibrosis and may serve as non-invasive indicators for diagnosis and characterization of renal fibrosis at clinical field strength.

### Conflicts of Interest

The authors have no potential conflicts of interest to disclose.

### Acknowledgments

The authors thank Xiaolei Song for MRI technical assistance (Russell H. Morgan Department of Radiology and Radiological Science, Johns Hopkins Medical Institutions, Baltimore, MD, USA).

### ORCID iDs

Zhen Li

<https://orcid.org/0000-0001-8037-4245>

Anqin Li

<https://orcid.org/0000-0001-6434-9488>

### REFERENCES

- Grenier N, Merville P, Combe C. Radiologic imaging of the renal parenchyma structure and function. *Nat Rev Nephrol* 2016;12:348-359
- Baues M, Dasgupta A, Ehling J, Prakash J, Boor P, Tacke F, et al. Fibrosis imaging: current concepts and future directions. *Adv Drug Deliv Rev* 2017;121:9-26
- Vanhove T, Vermeulen T, Annaert P, Lerut E, Kuypers DRJ. High inpatient variability of tacrolimus concentrations predicts accelerated progression of chronic histologic lesions in renal recipients. *Am J Transplant* 2016;16:2954-2963
- Nastase MV, Zeng-Brouwers J, Wygrecka M, Schaefer L. Targeting renal fibrosis: mechanisms and drug delivery systems. *Adv Drug Deliv Rev* 2018;129:295-307
- Morrell GR, Zhang JL, Lee VS. Magnetic resonance imaging of the fibrotic kidney. *J Am Soc Nephrol* 2017;28:2564-2570
- Togao O, Doi S, Kuro-o M, Masaki T, Yorioka N, Takahashi M. Assessment of renal fibrosis with diffusion-weighted MR imaging: study with murine model of unilateral ureteral

- obstruction. *Radiology* 2010;255:772-780
7. Boor P, Perkuhn M, Weibrecht M, Zok S, Martin IV, Gieseke J, et al. Diffusion-weighted MRI does not reflect kidney fibrosis in a rat model of fibrosis. *J Magn Reson Imaging* 2015;42:990-998
  8. Inoue T, Kozawa E, Okada H, Inukai K, Watanabe S, Kikuta T, et al. Noninvasive evaluation of kidney hypoxia and fibrosis using magnetic resonance imaging. *J Am Soc Nephrol* 2011;22:1429-1434
  9. Woo S, Cho JY, Kim SY, Kim SH. Intravoxel incoherent motion MRI-derived parameters and T2\* relaxation time for noninvasive assessment of renal fibrosis: an experimental study in a rabbit model of unilateral ureter obstruction. *Magn Reson Imaging* 2018;51:104-112
  10. Clatworthy MR, Kettunen MI, Hu DE, Mathews RJ, Witney TH, Kennedy BW, et al. Magnetic resonance imaging with hyperpolarized [1,4-<sup>13</sup>C<sub>2</sub>]fumarate allows detection of early renal acute tubular necrosis. *Proc Natl Acad Sci U S A* 2012;109:13374-13379
  11. Laustsen C, Lycke S, Palm F, Østergaard JA, Bibby BM, Nørregaard R, et al. High altitude may alter oxygen availability and renal metabolism in diabetics as measured by hyperpolarized [1-<sup>13</sup>C]pyruvate magnetic resonance imaging. *Kidney Int* 2014;86:67-74
  12. Takahashi T, Wang F, Quarles CC. Current MRI techniques for the assessment of renal disease. *Curr Opin Nephrol Hypertens* 2015;24:217-223
  13. van Zijl PCM, Lam WW, Xu J, Knutsson L, Stanisz GJ. Magnetization transfer contrast and chemical exchange saturation transfer MRI. Features and analysis of the field-dependent saturation spectrum. *Neuroimage* 2018;168:222-241
  14. Su C, Zhao L, Li S, Jiang J, Cai K, Shi J, et al. Amid proton transfer (APT) and magnetization transfer (MT) MRI contrasts provide complimentary assessment of brain tumors similarly to proton magnetic resonance spectroscopy imaging (MRSI). *Eur Radiol* 2019;29:1203-1210
  15. Jiang K, Ferguson CM, Ebrahimi B, Tang H, Kline TL, Burningham TA, et al. Noninvasive assessment of renal fibrosis with magnetization transfer MR imaging: validation and evaluation in murine renal artery stenosis. *Radiology* 2017;283:77-86
  16. Zhang H, Kang H, Zhao X, Jiang S, Zhang Y, Zhou J, et al. Amide proton transfer (APT) MR imaging and magnetization transfer (MT) MR imaging of pediatric brain development. *Eur Radiol* 2016;26:3368-3376
  17. Adler J, Swanson SD, Schmiedlin-Ren P, Higgins PD, Golembeski CP, Polydorides AD, et al. Magnetization transfer helps detect intestinal fibrosis in an animal model of Crohn disease. *Radiology* 2011;259:127-135
  18. Jiang K, Ferguson CM, Woollard JR, Zhu X, Lerman LO. Magnetization transfer magnetic resonance imaging noninvasively detects renal fibrosis in swine atherosclerotic renal artery stenosis at 3.0 T. *Invest Radiol* 2017;52:686-692
  19. Liu G, Song X, Chan KW, McMahon MT. Nuts and bolts of chemical exchange saturation transfer MRI. *NMR Biomed* 2013;26:810-828
  20. Wang F, Kopylov D, Zu Z, Takahashi K, Wang S, Quarles CC, et al. Mapping murine diabetic kidney disease using chemical exchange saturation transfer MRI. *Magn Reson Med* 2016;76:1531-1541
  21. Wen Z, Hu S, Huang F, Wang X, Guo L, Quan X, et al. MR imaging of high-grade brain tumors using endogenous protein and peptide-based contrast. *Neuroimage* 2010;51:616-622
  22. Jin Y, Liu R, Xie J, Xiong H, He JC, Chen N. Interleukin-10 deficiency aggravates kidney inflammation and fibrosis in the unilateral ureteral obstruction mouse model. *Lab Invest* 2013;93:801-811
  23. Zhao Y, Yin Z, Li H, Fan J, Yang S, Chen C, et al. MiR-30c protects diabetic nephropathy by suppressing epithelial-to-mesenchymal transition in db/db mice. *Aging Cell* 2017;16:387-400
  24. Wang F, Takahashi K, Li H, Zu Z, Li K, Xu J, et al. Assessment of unilateral ureter obstruction with multi-parametric MRI. *Magn Reson Med* 2018;79:2216-2227
  25. Padovano V, Podrini C, Boletta A, Caplan MJ. Metabolism and mitochondria in polycystic kidney disease research and therapy. *Nat Rev Nephrol* 2018;14:678-687
  26. van Zijl PC, Yadav NN. Chemical exchange saturation transfer (CEST): what is in a name and what isn't? *Magn Reson Med* 2011;65:927-948
  27. Zu Z. Towards the complex dependence of MTR<sub>asym</sub> on T1<sub>w</sub> in amide proton transfer (APT) imaging. *NMR Biomed* 2018;31:e3934
  28. Takahashi M, Kume H, Koyama K, Nakagawa T, Fujimura T, Morikawa T, et al. Preoperative evaluation of renal cell carcinoma by using 18F-FDG PET/CT. *Clin Nucl Med* 2015;40:936-940
  29. Pijl JP, Glaudemans AWJM, Slart RHJA, Kwee TC. <sup>18</sup>F-FDG PET/CT in autosomal dominant polycystic kidney disease patients with suspected cyst infection. *J Nucl Med* 2018;59:1734-1741
  30. Epelboym Y, Shyn PB, Chick JFB, Hamilton MJ, O'Connor SD, Silverman SG, et al. Crohn disease: FDG PET/CT before and after initial dose of anti-tumor necrosis factor therapy to predict long-term response. *Clin Nucl Med* 2017;42:837-841
  31. Cho A, Chung YE, Lee JH, Yun M, Lee JD, Kang WJ. Evaluation of <sup>18</sup>F-FDG excretion patterns in malignant obstructive uropathy. *Clin Nucl Med* 2013;38:695-702
  32. Jadoul A, Lovinfosse P, Weekers L, Delanaye P, Krzesinski JM, Hustinx R, et al. The uptake of <sup>18</sup>F-FDG by renal allograft in kidney transplant recipients is not influenced by renal function. *Clin Nucl Med* 2016;41:683-687
  33. Liu Y. Cellular and molecular mechanisms of renal fibrosis. *Nat Rev Nephrol* 2011;7:684-696
  34. Zhang XY, Wang F, Li H, Xu J, Gochberg DF, Gore JC, et al. CEST imaging of fast exchanging amine pools with corrections for competing effects at 9.4 T. *NMR Biomed* 2017;30:e3715